Characterization and Comparison of GaAs/AlGaAs Uni-Traveling Carrier and Separated-Transport-Recombination Photodiode Based High-Power Sub-THz Photonic Transmitters

Yu-Tai Li, Jin-Wei Shi, *Member, IEEE*, C.-Y. Huang, Nan-Wei Chen, Shu-Han Chen, *Member, IEEE*, Jen-Inn Chyi, *Senior Member, IEEE*, Yi-Chao Wang, Chan-Shan Yang, and Ci-Ling Pan, *Senior Member, IEEE*

***Abstract*—We describe in detail the characterization of two high-power photonic transmitters based on two different kinds of high-power photodiodes, one a GaAs/AlGaAs based uni-traveling-carrier photodiode (UTC-PD) and the other a separated-transport-recombination photodiode (STR-PD). The diodes operate under optical pulse excitation at the 800 nm wavelength. Both PDs have the same total depletion layer thickness (same theoretical RC-limited bandwidth) and are monolithically integrated with the same broadband micro-machined circular disk monopole antennas to radiate strong sub-THz pulses. However the STR-PD based transmitter exhibits very different dynamic and static performance from that of the UTC-PD based transmitter due to the existence of a low-temperature-grown GaAs (LTG-GaAs) based recombination center inside the active region, and the much thinner thickness of effective depletion layer. Under optical pulse excitation ($\sim$480 pJ/pulse), the STR-PD based transmitter exhibits a much lower maximum averaged output photocurrent (1.2 mA versus 0.3 mA) than that of the UTC-PD transmitter, although the radiated electrical pulse-width and maximum peak-power, which are measured by the same THz time-domain spectroscopic (TDS) system, of both devices are comparable. These results indicate that although the recombination center in the STR-PD degrades its DC responsivity, it effectively improves the high-speed and output power performance of the device and eliminates the DC component of the photocurrent, which should minimize device-heating problem during high-power operation. The radiated waveforms of both devices under intense optical pulse illumination also exhibit excellent linearity and strong bias dependent magnitude. This suggests their suitability for application as photonic emitters and possibly as a data modulator in sub-THz impulse-radio communication systems.**

***Index Terms*—High-power photodiode, uni-traveling carrier photodiode (UTC-PD), separated-transport recombination photodiode (STR-PD), photonic transmitter, submillimeter-wave, terahertz (THz).**

Manuscript received March 09, 2009; revised April 24, 2009. Current version published December 04, 2009. This work was supported in part by the National Science Council (NSC) of Taiwan through various grants including PPAEU-II, and the Ministry of Education's ATU program, Taiwan.

Y.-T. Li, Y.-C. Wang, and C.-S. Yang are with the Department of Photonics, National Chiao-Tung University, Hsinchu 300, Taiwan.

J.-W. Shi, C.-Y. Huang, N.-W. Chen, S.-H. Chen, and J.-I. Chyi are with the Department of Electrical Engineering, National Central University, Taoyuan 32001, Taiwan (e-mail: jwshi@ee.ncu.edu.tw).

C.-L. Pan was with the Department of Photonics, National Chiao-Tung University, Hsinchu, Taiwan, and is now at the Department of Physics and Institute of Photonics Technologies, National Tsing-Hua University, Hsinchu 30013, Taiwan (e-mail: clpan@phys.nthu.edu.tw).

Color versions of one or more of the figures in this paper are available online at http://ieeexplore.ieee.org.

Digital Object Identifier 10.1109/JQE.2009.2023366

I. INTRODUCTION

RECENTLY, THz technology has attracted a considerable amount of attention, because of its increasing variety of applications, ranging from communications, security screening to medicine and nondestructive evaluation [1]. These applications need compact, convenient, broadband THz sources with high output power. Some proposed applications include sub-THz sources, Gunn diodes, resonant tunneling diodes [2], [3], and quantum cascade THz lasers [4]–[6]. Currently, several related products like THz image systems, THz spectroscopy kits, etc.[12] are now commercially available. These systems usually constructed with Ti:sapphire mode-locked laser ($\lambda = 800$ nm) and compact THz emitter modules. It is attractive to replace these modules by compact photonic-transmitters (PTs), which are composed of an antenna and a high speed and power photodiode (PD) [7]–[10]. The PTs have the advantages of simplicity, room-temperature operation, tunable THz wavelength, and easy integrability with other semiconductor devices.

In addition, under optical excitation with short pulse lasers or heterodyne-beating continuous-wave (CW) laser diodes, PTs can also efficiently radiate pulse or CW THz waves. PTs can also provide an interesting alternative for wireless communication link applications. As we know, the demand for high-bit-rate wireless local area networks has grown rapidly. Impulse radio (IR) is one technology that has been proposed to meet this demand. However, there remain considerable challenges to be overcome for IR applications [11]. For example, there is huge propagation loss in free-space of short (sub-picoseconds) electrical pulses, which may directly be generated by electronic devices such as nonlinear transmission lines [12]. This type of problem could be overcome by the use of photonic technology in an IR system, where the optical pulse signal is distributed through a low-loss optical fiber and an optical-pulse triggered PT is utilized to radiate the converted electrical signal to the user-end over the last-mile.

[1]The kit is supported by EKSPLA Corp., Lithuania, www.ekspla.com.

[2]The kit is supported by Picometrix Inc., USA, www.picometrix.com.

0018-9197/$26.00 © 2009 IEEE

Some PT-based sub-terahertz (sub-THz) IR communication links have also been demonstrated [13]–[15]. In order to further improve the maximum transmission distance, it is necessary to have a PD which can sustain its high-speed performance and deliver high output power under intense optical pulse excitation. There are two major strategies to meet this challenge [16]. One is to distribute and make uniform the photocurrents along edge-coupled PDs by improving the structure of optical and electrical waveguides, for example, the velocity matched distributed photodetector (VMDP) [17] and evanescent coupled photodiode (ECPD) [18], [19]; the other strategy involves minimizing the space-charge screening (SCS) effect [16], [20] in the photo-absorption volume. Under intense optical power illumination, the photo-generated carriers will induce a strong space-charge field, screen out the external applied electrical field, and seriously limit the output saturation power of the PD.

By increasing the drift-velocity of photo-generated carriers, such as with the structure of a uni-traveling carrier PD (UTC-PD), is one way to minimize the SCS effect. Excellent high-speed and high-power performance has been demonstrated [21] in UTC-PD.

Under 1.55 μm long wavelength excitation, an InP/InGaAs based UTC-PD based photonic-transmitter has been shown to generate a continuous wave (CW) output power at 1.04 THz of as high as 2.3 μW [7], [21]. In the case of an InP based UTC-PD operated under 0.8 μm wavelength excitation, the incident photon will have enough photon energy to induce the absorption process in the InP based collector layer. The presence of photo-generated holes in the collector layer will degrade the high-power performance of the UTC-PD. We overcome this problem with our demonstrated high-speed GaAs/AlGaAs based UTC-PD [22], which is composed of a GaAs based p-type photo-absorption layer and an $Al_{0.15}Ga_{0.85}As$ based collector layer. Undesired photo-absorption under 800 nm wavelength excitation is avoided with this device. We have also demonstrated a high-power photonic-transmitter that operates under 800 nm optical short-pulse excitation [23].

It is also possible to minimize the SCS effect by decreasing the thickness of the depletion layer which has a direct effect on the carrier transit time, such as the structure of a partially depleted absorber photodiode [24]. However, PDs with thin depletion layers usually suffer from problems of low quantum efficiency and very limited *RC* bandwidth. In order to overcome the above-mentioned problems, we have demonstrated a p-i-n photodiode structure: the Separated-Transport-Recombination photodiode (STR-PD), which can greatly relieve the trade-off between output saturation power, quantum efficiency, and electrical bandwidth performance [25]. In the demonstrated GaAs based STR-PD, a LTG-GaAs layer is adopted, which has an extremely short carrier lifetime (less than 1 ps) [26], to serve as the recombination center in the active photo-absorption region. The STR-PD exhibits superior electrical bandwidth performance under a higher output current regime without seriously sacrificing responsivity compared to that of the control p-i-n PD (with a pure intrinsic GaAs based photo-absorption layer) [25]. The integration of the STR-PD with a narrowband slot-antenna to produce an STR-PD based photonic transmitter has been described previously [27].

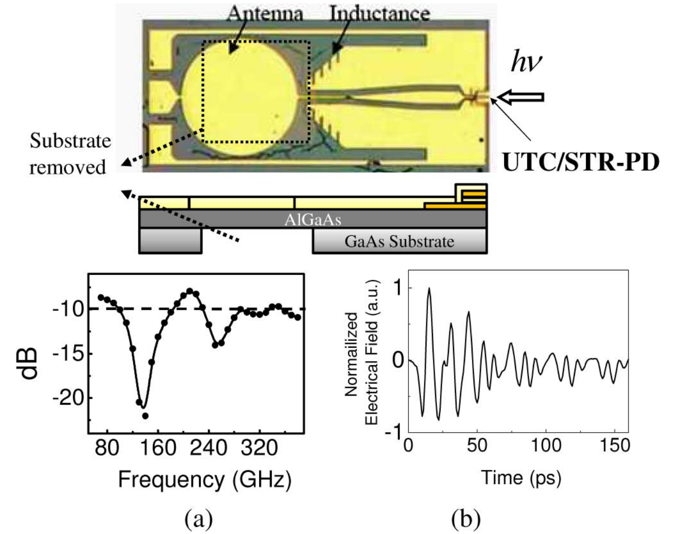

Fig. 1. Top-view and cross-sectional view of the demonstrated sub-THz PT. Inset (a) shows the simulated frequency response of the designed antenna. Inset (b) shows the simulated impulse response of the antenna.

In this study, we integrate two different kinds of high-power photodiodes (UTC-PD and STR-PD) with the same type of planar antenna (circular disk monopole antenna) to serve as photonic transmitters. We compare their dynamic performance using the same THz time-domain spectroscopic system. These two different devices exhibit distinct dynamic behaviors and very different mechanisms of saturation. Under high optical pulse energy excitation ($\sim$480 pJ/pulse), the STR-PD based transmitter exhibits much a lower maximum average output photocurrent (1.2 mA versus 0.3 mA) than that of the UTC-PD transmitter. The radiated electrical envelop-width ($\sim$50 ps) and maximum peak-power ($\sim$9 mW) of both devices are comparable. This indicates that although the DC responsivity in the STR-PD is degraded, the high-speed and output power performance of this device has been effectively improved and the DC component of the photocurrent eliminated. The smaller DC photocurrent implies that device-heating problems of STR-PD based transmitters during high-power operation will be decreased. The dynamic measurement results reveal that although the working principles for the high-power performance of the STR-PD and UTC-PD are totally different, both devices exhibit comparable and promising high-speed and high-power performance for applications in THz photonic transmitters.

II. Device Structure

To make a fair comparison of their dynamic performance, both the STR-PD and UTC-PD based transmitters share the same geometric structure. A top-view and conceptual cross-sectional view are shown in Fig. 1. The antenna design adopted in this work is a co-planar-waveguide (CPW) fed circular disk monopole antenna [28]. As can be seen in the cross-sectional view, part of the GaAs substrate of both devices just below the circular disk of the antenna has been removed by selective wet etching and back-side lithography to enhance the THz emission of the emitter without necessitating the integration of an additional Si-lens [29]. Furthermore, a tapered and periodically corrugated edge, which is specified for inductance, can be seen on

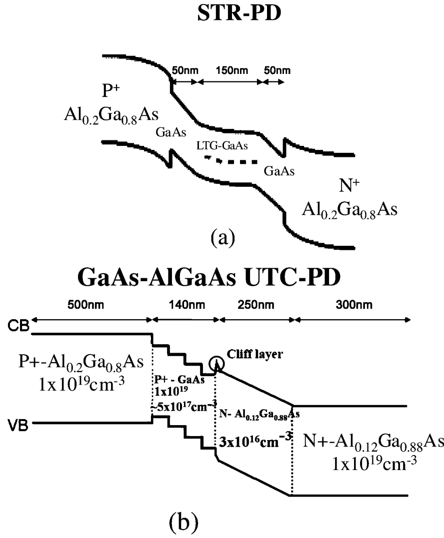

Fig. 2. Conceptual band diagrams of the demonstrated (a) STR-PD and (b) UTC-PD.

the top-view of the device. A circular disk antenna is integrated to improve the radiation characteristics, particularly at frequencies near the higher band edge [28].

Inset (a) to Fig. 1 shows the simulated frequency response of the microwave reflection parameter (S_{11}) for the antenna structure. By using the -10 dB line on the y axis as a reference it can be seen that there is low reflection loss (< -10 dB) for most of the frequency component (100 GHz to 350 GHz) in the simulated frequency band (70 GHz to 350 GHz) [23]. The inset (b) shows the simulated waveforms for the radiated electrical pulse from our substrate-removed antenna. The electrical pulse from the photodiode is considered Gaussian in shape with a full-width half maximum (FWHM) around 4 ps. The simulation is carried out with a finite-difference time-domain simulation tool (SEMCAD, Schmid & Partners Engineering. AG, Zurich, Switzerland).

Fig. 2 shows conceptual band diagrams of the demonstrated STR-PD and UTC-PD [22], [25]. In the STR-PD, a LTG-GaAs layer with a short carrier lifetime (less than 1 ps) is inserted into the center of the absorption region and surrounded by two high quality GaAs-based photo-absorption layers to serve as a recombination center. As shown in Fig. 2(a), the external applied electric field is concentrated in the two GaAs layers. This is due to the high defect density and field-screening effect of the inserted LTG-GaAs layer [25]. These two photo-absorption layers can, thus, be treated as a “transport layer” or “depletion layer” in our structure. They have much higher mobility compared to the LTG-GaAs and the concentration of the applied electric field. The STR-PD demonstrates superior output power performance over that of the traditional p-i-n PD even though the thickness of the total absorption layer is the same [25]. This is due to the fact that in the STR-PD the real drift-distance of photo-generated carriers can be roughly approximated by the thickness of the one-sided GaAs based transport layer (a thickness of only 50 nm) instead of the total absorption region (with a thickness of up to 250 nm). A smaller drift-distance means that a shorter drift-time, less SCS effect in the absorption region, and a higher saturation power can be expected [16]. Furthermore, the inserted LTG-GaAs based recombination center has high resistivity, which can also reduce the junction capacitance (RC-limited bandwidth) over that of the traditional p-i-n PD with its thin absorption (depletion) layer for high-power performance [25].

The UTC-PD is composed of a GaAs based photo-absorption layer with a graded p-type doping profile, which acts to accelerate the drift-velocity of the photo-generated electrons [22] and the $Al_{0.15}Ga_{0.85}As$ based collector layer. The graded doping profile of the absorption layer has a larger slope, which induces the appropriate built-in electric field (2.1 to 84 kV/cm) and ensures the occurrence of electron drift for the over-shoot velocity. Thus, our UTC-PD has a more significant bandwidth enhancement effect under a much lower output photocurrent density than the traditional InP based UTC-PD [22]. The collector layer consists of an n-type doped (3×10^{16} cm^{-3}) $Al_{0.15}Ga_{0.85}As$ layer, 250 nm in thickness, with a bandgap of around 1.61 eV. This enables one to avoid the undesired photo-absorption process that occurs around the 800 nm wavelength excitation. The n-type doping in the collector layer can also suppress the current blocking effect and further improve the high power performance of UTC-PD [16]. An n^+ doped (5×10^{18} cm^{-3}) $Al_{0.15}Ga_{0.85}As$ cliff layer with a 20 nm thickness is inserted between the collector layer and the absorption layer [21]. A UTC-PD structure that utilizes only electrons as the active carriers has superior high-power performance to the traditional p-i-n PD due to the much higher drift-velocity of the electrons than of the holes, and the great reduction in the drift-time of the photo-generated carriers. In short, we use different approaches to shorten the drift-time of photo-generated carriers: one approach is the reduction of the effective carrier drift-distance in the STR-PD and the other is the increasing of the drift-velocity in the UTC-PD. Both of these structures exhibit superior high-power performance over that of a p-i-n PD with the same total depletion layer thickness [21], [22], [25].

III. Measurement Results and Discussion

During device testing, an objective lens with a high numerical aperture (NA) value is used to focus the output of the fs Ti:Sappire mode-locked laser ($\lambda = 800$ nm) onto the edge of our devices. The excitation optical pulse has a repetition rate of 82 MHz and a pulsewidth of 100 fs. Fig. 3(a) and (b) shows the bias current versus voltage (I-V) of the two devices under different input powers. The active lengths of the measured UTC-PD and STR-PD based PTs (UTC-PT and STR-PT) is the same, around 23 μm.

As can be seen in Fig. 3, the average photocurrent generated by the UTC-PT is much higher than that of the STR-PT, even under lower bias and input pulse energy. This can be attributed to the presence of the LT-GaAs based recombination center inside the STR-PD active layers, which effectively traps the photo-generated carriers and degrades the external quantum efficiency of the device. The generated photocurrent of the UTC-PT increases super-linearly with the reverse bias voltage when it is over 5 V. This phenomenon can be attributed to the fact that the value of the external applied electrical field (3.6×10^5 V/cm)

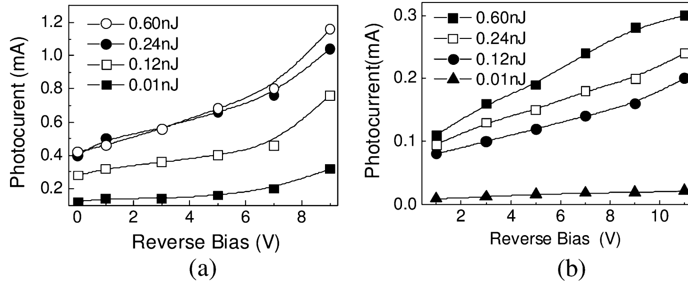

Fig. 3. Comparison of bias dependent photo-currents of (a) UTC-PT and (b) STR-PT devices with the same absorption length of around 23 μm.

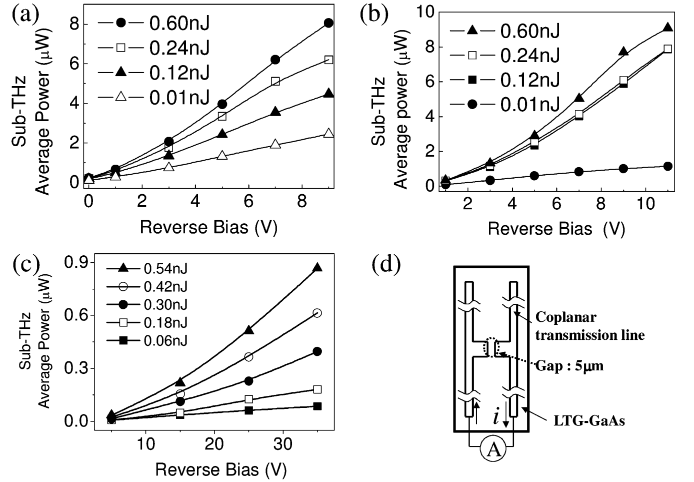

Fig. 4. The bias dependent measured sub-THz power of (a) UTC-PT, (b) STR-PT, and (c) LTG-GaAs based PC under different optical pulse energy excitation. (d) shows the top-view of PC dipole antenna.

in the $Al_{0.12}Ga_{0.88}As$ based collector layer is close to its breakdown field. In addition, considering the thin N^{+}AlGaAs based cliff layer, as shown in Fig. 2(b), with a 20 nm thickness and heavily doping level (5×10^{18} cm^{-3}), it could be expected that most of the breakdown phenomenon happens in such region due to its much higher doping density and lower critical field than those of other parts in the collector layer.

A super-linear increase of photocurrent versus reverse bias voltage has also been observed for the LTG-GaAs based PD [30], [31], which can be attributed to the lifetime increasing effect of LTG-GaAs layer. However, such phenomenon is much less apparent for our STR-PD, perhaps because most of the external electric field is concentrated in the two high quality GaAs transport layers instead of the LTG-GaAs based recombination center, which has a high defect density and field-screening effect under reverse bias voltages [25]. The lifetime increasing effect can thus be neglected. In addition, the avalanche induced photocurrent in the transport layers is not as significant as the case shown in Fig. 3(a), which may be attributed to the fact that most of the avalanche-generated carriers are also trapped by the recombination centers. Based on these measurement results, we can thus obtain the external quantum efficiencies of our devices. For UTC-PD, under -5 V bias while the breakdown phenomenon is not significant, the measured quantum efficiency is around 31% (0.16 mA photocurrent with 0.8 mW averaged optical power (0.01 nJ)). After considering the optical reflecting loss between air and input facet, the ideal external quantum efficiency of UTC-PD can be as high as 75%. Similarly, for the STR-PD, the measured quantum efficiency is around 4.2%, which is measured under 0.8 mW averaged optical power and -11 V bias voltage. The theoretical quantum efficiency of STR-PD can roughly be evaluated by using the ratio of carrier life-time over drift-time in LTG-GaAs layer. By assuming a 0.2 ps carrier lifetime [26] and a 1×10^{5} m/sec drift-velocity in LTG-GaAs layer, the theoretical external efficiency is around 10% after considering the optical reflection loss (75%).

As can be seen, the measured external quantum efficiencies (31% and 4.2%) of both UTC-PD and STR-PD are around 40% of their theoretical values (75% and 10%). The same difference between measured and theoretical efficiencies of two devices can be attributed to the optical propagation loss of ridge waveguides and the coupling loss of optical modes between ridge waveguide and launched optical wave.

The total output power of the two devices was measured by a liquid-Helium cooled Si bolometer, which was carefully calibrated to the black body source. Two parabolic mirrors were used to collimate and focus the generated sub-THz into the bolometer. The propagation loss (0.082 cm^{-1}) is also calibrated by measuring the THz intensity as a function of the propagation distance at a relative humidity of 40%. Fig. 4(a) and (b) shows plots of the sub-THz power of UTC-PT and STR-PT emitted under different optical pumping pulse energies as a function of the bias voltage. As much as 8 μW and 9 μW of maximum sub-THz average power are measured for the STR- and UTC-PT respectively. We can clearly see that although the maximum average photocurrent of the UTC-PT is around four times higher than that of the STR-PT, as shown in Fig. 3, the maximum average sub-THz power generated by the STR-PT is similar to that of the UTC-PT under a lower excitation optical pulse energy (0.12 nJ versus 0.48 nJ). This result indicates that the recombination center in the STR-PD has eliminated most of the DC component of the photocurrent, so the AC component of the optical pulses can be efficiently converted to an electrical AC signal and then radiated into free-space. The STR-PD requires less operation current for the desired radiated power performance which implies that the thermal effect can be minimized during high-power operation.

In addition, as shown in 4(a), when the reverse bias of UTC-PD is less than about -5 V, the radiated sub-THz power exhibits an ideal quadratic relation to the reverse bias voltage. This is due to the linear dependence of the output photocurrent on the reverse bias voltage (<-5 V), as shown in Fig. 3(a). When the reverse bias voltage increases further, however, the output sub-THz power exhibits a linear dependence on the bias voltage. This can be attributed to the fact that the value of the external applied electrical field ($\sim 3.6 \times 10^{5}$ V/cm) in the $Al_{0.12}Ga_{0.88}As$ based collector layer is close to its breakdown field. Thus, the avalanche-induced bandwidth degradation phenomenon of the PD limits the super-linear increase of output power versus the bias.

As can be seen in Fig. 3(a), the measured photocurrent clearly increases super-linearly with the bias voltage when it is over -5 V. This indicates that the avalanche phenomenon really does occur. The bias dependent output power of STR-PT shows similar behavior to the measured bias dependent photocurrent, as

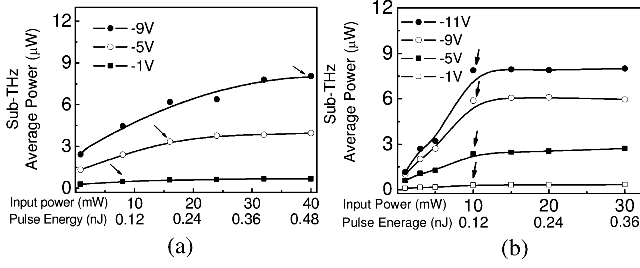

Fig. 5. The power dependent measured sub-THz power of (a) UTC-PT and (b) STR-PT under different reverse bias voltage.

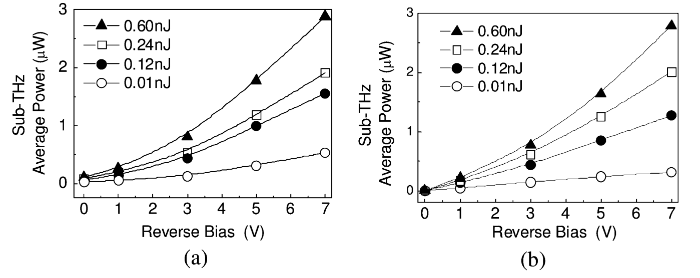

Fig. 6. Bias dependent sub-THz power of (a) UTC-PT and (b) STR-PT with a longer active length of 60 μm under different injected optical pulse energy.

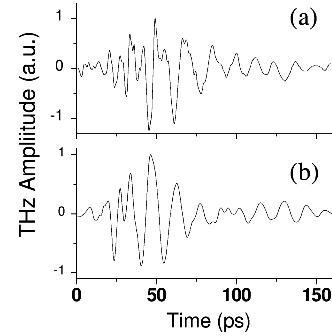

Fig. 7. The radiated waveform of sub-THz pulses for (a) UTC-PT and (b) STR-PT.

shown in Fig. 3(b). When the injected pulse energy increases from 0.01 nJ to 0.12 nJ, the emitted sub-THz power dramatically increases due to the huge increase of photocurrent; see Fig. 3(b). However, when the pulse energy exceeds 0.12 nJ, the traces under higher injected pulse energy are crowded due to the phenomenon of recombination center saturation, which will be discussed latter in Fig. 5.

Fig. 4(c) shows the measured bias dependent output sub-THz power from a typical photoconductive (PC) dipole antenna, which is fabricated on the LTG-GaAs layer [32] and mounted on the Si-lens. Such PT has a center frequency at 260 GHz with around 1 THz bandwidth. The measured values of power are close to those reported for an LTG-PC with an antenna of the same design [32]. Fig. 4(d) shows the top-view and geometric size of such device. We can clearly see that both of our devices can have around 10 times higher output sub-THz power than such LTG-GaAs based traditional PT by use of a much lower reverse bias voltage ($\sim$10 V versus 35 V).

Fig. 5(a) and (b) shows the measured optical power dependent output sub-THz power under different reverse bias voltage of UTC-PT and STR-PT, respectively. As can be seen, the value of the saturated injected optical pulse energy of the UTC-PT [indicated by arrows in Fig. 5(a)] increases with the reverse bias voltage. The observed saturation phenomenon of the UTC-PD should be attributed to the electron induced SCS effect in the collector layer [21], which can be minimized by increasing the reverse DC bias voltage [16], [21]. On the other hand, the power dependent saturation behavior of the STR-PD is very different from that of the UTC-PD [indicated by arrows in Fig. 5(b)]. We can clearly see that the saturation of the optical pulse energy is the same around 0.12 nJ regardless of an increase in the reverse bias voltage. This phenomenon may be attributed to that fact that the dominant saturation mechanism in the STR-PD is the defect saturation of the LTG-GaAs based recombination center, rather than the SCS effect when the effective depletion (transport) layer is as thin as 50 nm. The external applied reverse bias voltage is concentrated in the transport layers and thus has no influence on the saturation point of the recombination centers. The results of the optical simulation show that the coupling efficiency between the injected beam (beam diameter of around 2 μm) and the active waveguide of the STR-PD is around 30%. We can thus roughly estimate that the photo-generated carrier density under 0.12 nJ pulse energy excitation is as high as $\sim 1 \times 10^{19}$ cm^{-3}. This value is close to the reported defect density of the LTG-GaAs material [33].

Fig. 6(a) and (b) shows plots of the bias dependent emitted sub-THz power of UTC-PT and STR-PT with the same waveguide width and a longer active length ($\sim$60 μm) than that of the measured devices ($\sim$20 μm) as discussed in Figs. 4 and 5. We can clearly see that due to the longer active lengths and poor RC-limited bandwidth, both devices exhibit less than one-half of the maximum output power than that shown in Fig. 5 under the same reverse bias voltage and input pulse energy.

We utilized a THz-TDS system [14] to investigate the waveform of the radiated sub-THz impulse that could be applied to the IR communication system. The same mode-locked Ti:sapphire laser was used to pump both devices. The injected optical pulse energy was 480 pJ/pulse. A photo-conductive (PC) dipole antenna, as shown in Fig. 4(d), fabricated on a LTG-GaAs layer and integrated with a Si-lens is used to probing the radiated signal. The direction of the dipole antenna was adjusted parallel to the direction of the polarization of the radiated sub-THz pulses. With identical PC antenna as the emitter and receiver, our THz-TDS system exhibits a bandwidth exceeding 1 THz and a signal-to-noise ratio better than 1000.

Fig. 7(a) and (b) shows the measured waveforms of the radiated sub-THz pulses of UTC-PT and STR-PT under the same reverse bias voltage (-9 V), respectively. The corresponding fast Fourier transform (FFT) spectra of UTC-PT and STR-PT are shown in Fig. 8(a). The measured waveform and corresponding FFT spectrum of adopted LTG-GaAs PC antenna is shown in (b) for reference. As can be seen in Fig. 7, the shapes of the measured pulses in the time domain are similar for STR-PT and UTC-PT. The measured traces show a fast oscillation period with a slow-varying envelope, which has an envelope with of around 100 ps. The full-width-half-maximums (FWHMs) of the main peaks of the oscillating waveforms are around 3.9 ps

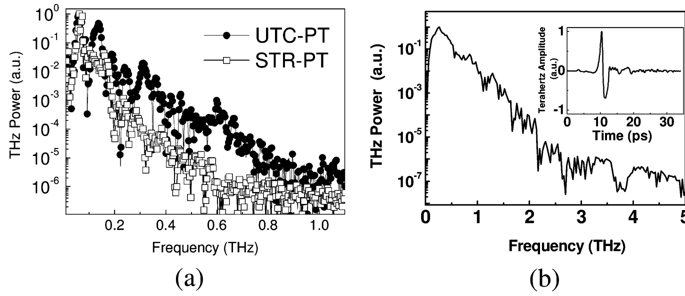

Fig. 8. The normalized power spectrum of (a) UTC-PT, STR-PT and (b) LTG-GaAs based PC antenna. The inset shows the measured waveform of PC antenna.

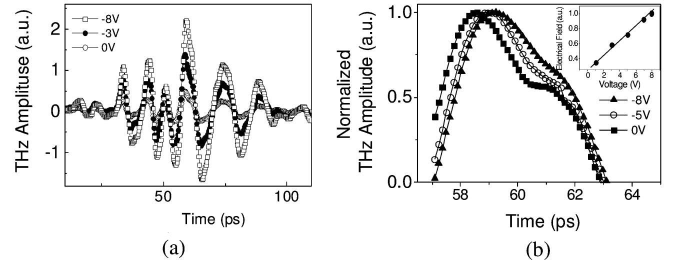

Fig. 9. Bias dependent waveforms of the radiated sub-THz pulses for (a) UTC-PT and (b) the normalized and enlarged main peak. The inset shows the normalized peak values versus reverse bias.

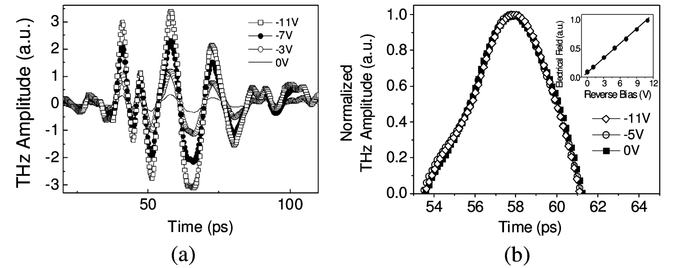

Fig. 10. Bias dependent waveforms of the radiated sub-THz pulses for (a) STR-PT and (b) the normalized and enlarged main peak. The inset shows the normalized peak values versus reverse bias.

and 4.4 ps for UTC-PT and STR-PT, respectively. As shown in Fig. 8(a), the bandwidth of both devices cover from near DC to around 250 GHz. We defined the bandwidth of device as its THz power drops to around 10^{-2}, as shown in the y axis of Fig. 8(a). When the operating frequency is over 250 GHz, a serious high-frequency roll-off has been observed in both devices, which may be attributed to the limited optical-to-electrical (O-E) bandwidths of integrated PDs. We have calculated the theoretical 3-dB O-E bandwidths of integrated UTC-PD and STR-PD. The bandwidth calculation of UTC-PD can be referred to [21], [22], [34]. In our calculation, we assumed a 5000 cm^2/V-sec mobility and a 4.4×10^5 m/sec thermal velocity (V_{th}) of electron in the p-type GaAs absorption layer and a 1.5×10^5 m/sec drift-velocity of electron in the AlGaAs based collector layer. With respect to the STR-PD, its theoretical bandwidth calculation can be referred to our previous work [35]. Here, we assumed that the carrier life-time in LTG-GaAs layer is around 200 fs [26], [35]. In our bandwidth calculations, we also included the 50 Ω load resistance and RC-limited bandwidths of both devices, which can be derived from the measured microwave scattering (S) parameters. The calculated 3-dB bandwidth of UTC-PD and STR-PD is around 110 GHz and 105 GHz, respectively. Such calculated bandwidths are consistent with our FFT results as shown in Fig. 8(a). As can be seen, the frequency response starts to roll-off when the operating frequency is over 150 GHz due to the limited 3-dB bandwidth of both devices. More detailed experiments are necessary and will be performed in future to accurately extract the O-E 3-dB bandwidth of the two PDs.

The observed ringing (oscillation) is consistent with the simulation result, as shown in Fig. 1(b), and can be attributed to the influence of the integrated antenna on the radiated impulse response. As a first approximation, the photo-generated electrical pulse from the UTC-PD can be considered to be Gaussian in shape. It exhibits a frequency response from the DC to hundreds of GHz. However, the integrated antenna functions like a "filter", in the sense, that it passes (radiates) a specific band of frequencies associated with the multi-resonance feature of the antenna structure. Hence, the frequency components outside the operating band of the antenna are suppressed in the radiated field, which leads to the ringing of the measured pulse. Observed ringing can also be attributed to multiple reflections between the substrate-removed antenna and chip boundaries, where the GaAs substrate has not been removed. Similar phenomena have been reported for InP UTC-PD based photonic transmitters and explained by the same mechanism [36].

TABLE I
LIST OF MEASUREMENT RESULTS OF UTC-PT AND STR-PT

	UTC-PT	STR-PT
Envelope FWHM	47.2ps	57.0ps
FWHM of main pulse	3.9ps	4.4ps
Max average power	8μW	9μW
Peak power	9.2mW	7.8mW
Experimental Bandwidth	250GHz	200GHz

By use of the square of measured electrical field waveform as shown in Fig. 7, we can get normalized waveform of radiated power in time domain. The integration of such waveform with time could be written as a function of peak power value, which equals to the measured average sub-THz power divided by repetition rate of pulses. As a result, with the parameters of measured average power and repetition rate of pulses, peak power could thus be obtained. The measured and calculation results are shown in detail in Table I. We can clearly see that the STR-PT has a comparable radiated peak-power ($\sim$9.2 mW), and FFT bandwidth ($\sim$250 GHz) under a much lower operation current than does the UTC-PT. By using the bias modulation technique, a photonic transmitter could serve as a sub-THz emitter and data modulator [37], [38]. As a result, we measure the bias dependent sub-THz waveforms of both devices in detail using the same THz-TDS system. Figs. 9(a) and 10(a) show the measured waveforms for the UCT-PT and STR-PT under different reverse bias voltages and fixed optical pumping pulse energy ($\sim$480 pJ/pulse). Figs. 9(b) and 10(b) show the normalized main peak pulses for (a). We can clearly see that both devices exhibit excellent linearity, which means that the shape of the measured waveforms remain unchanged from zero-bias to high bias operation, even under high peak-power output ($\sim$8 mW) [39]. Fig. 9

shows the case for UTC-PT, where the bias voltage sweeps from 0 to 8 V, and the peak-electrical field increases about five times (0.5 to 2.4). The results for the STR-PT are shown in Fig. 10. Its peak-electrical field increases about 11 times (0.3 to 3.4) as the bias voltage sweeps from 0 to 11 V. These measurements results are an indication of the potential of these two devices to serve as sub-THz emitters and data modulators, using the bias modulation technique [37], [38] with much lower driving voltages than that of the traditional PC-antenna [14].

IV. Conclusion

We investigated in detail the dynamic behaviors of two high-power PTs, which were constructed by monolithically integrating GaAs/AlGaAs-based UTC-PDs and STR-PDs with the same substrate-removed monopole antenna, by use of the THz-TDS system. By shortening the effective carrier drift-distance and increasing the carrier drift-velocity in the STR-PD and UTC-PD we could obtain PT radiated sub-THz pulses with peak powers as high as 8 mW and a wide bandwidth (around 250 GHz). Furthermore, the output power performance and speed of the STR-PT were comparable to those of the UTC-PT under a much lower operation current, which may minimize the thermal problems encountered under high-power operation. The strong bias dependent high-peak-power performance and excellent linearity of these two devices suggests their suitability for application as photonic emitters and possibly as data modulators in sub-THz IR communication systems.

References

[1] M. Tonouci, "Cutting-edge terahertz technology," *Nat. Photon.*, vol. 1, pp. 97–105, Feb. 2007.

[2] H. Eisele, A. Rydberg, and G. I. Haddad, "Recent advances in the performance of InP gunn devices and GaAs TUNNET diodes for the 100–300-GHz frequency range and above," *IEEE Trans. Microw. Theory Tech.*, vol. 48, no. 4, pp. 626–631, Apr. 2000.

[3] N. Orihashi, S. Suzuki, and M. Asada, "One THz harmonic oscillation of resonant tunneling diodes," *Appl. Phys. Lett.*, vol. 87, p. 233501, 2005.

[4] R. Köhler, A. Tredicucci, F. Beltram, H. E. Beere, E. H. Linfeld, A. G. Davies, D. A. Ritchie, R. C. Iotti, and F. Rossi, "Terahertz semiconductor-heterostructure laser," *Nature*, vol. 417, pp. 156–159, May 2002.

[5] S. Barbieri, J. Alton, S. S. Dhillon, H. E. Beere, M. Evans, E. H. Linfield, A. G. Davies, D. A. Ritchie, R. Kohler, A. Tredicucci, and F. Beltram, "Continuous-wave operation of terahertz quantum-cascade lasers," *IEEE J. Quantum Electron.*, vol. 39, no. 4, pp. 586–591, Apr. 2003.

[6] C. Walther, M. Fischer, G. Scalari, R. Terazzi, N. Hoyler, and J. Faist, "Quantum cascade lasers operating from 1.2 to 1.6 THz," *Appl. Phys. Lett.*, vol. 91, p. 131122, Sep. 2007.

[7] H. Ito, T. Furuta, F. Nakajima, K. Yoshino, and T. Ishibashi, "Photonic generation of continuous THz wave using uni-traveling-carrier photodiode," *J. Lightw. Technol.*, vol. 23, p. 4016, 2005.

[8] M.-C. Tien, H.-H. Chang, J.-Y. Lu, L.-J. Chen, S.-Y. Chen, R.-B. Wu, W.-S. Liu, J.-I. Chyi, and C.-K. Sun, "Device saturation behavior of submillimeter-wave membrane photonic transmitters," *IEEE Photon. Technol. Lett.*, vol. 16, p. 873, 2004.

[9] S. Verghese, K. A. McIntosh, and E. R. Brown, "Highly tunable fiber-coupled photomixers with coherent terahertz output power," *IEEE Trans. Microw. Theory Tech.*, vol. 45, p. 1301, 1997.

[10] S. M. Duffy, S. Verghese, K. A. McIntosh, A. Jackson, A. C. Gossard, and S. Matsuura, "Accurate modeling of dual dipole and slot elements used with photomixers for coherent terahertz output power," *IEEE Trans. Microw. Theory Tech.*, vol. 49, no. 6, pp. 1032–1038, Jun. 2001.

[11] M. Z. Win and R. A. Scholtz, "Impulse radio: How it works," *IEEE Commun. Lett.*, vol. 2, no. 2, pp. 36–38, Feb. 1998.

[12] M. J. W. Rodwell, S. T. Allen, R. Y. Yu, M. G. Case, U. Bhattacharya, M. Reddy, E. Carman, M. Kamegawa, Y. Konishi, J. Pusl, and R. Pullela, "Active and nonlinear wave propagation devices in ultrafast electronics and optoelectronics," *Proc. IEEE*, vol. 82, no. 7, pp. 1037–1059, Jul. 1994.

[13] H. Togo, P.-C. P. Sah, N. Shimizu, and T. Nagatsuma, "Gigabit impulse radio link using photonic signal-generation techniques," in *Proc. Eur. Microwave Conf. 2005*, Oct. 2005, vol. 1, pp. 4–7.

[14] T.-A. Liu, G.-R. Lin, Y.-C. Chang, and C.-L. Pan, "Wireless audio and burst communication link with directly modulated THz photoconductive antenna," *Opt. Expr.*, vol. 13, no. 25, pp. 10416–10423, Dec. 2005.

[15] L. Möller, J. Federici, A. Sinyukov, C. Xie, H. C. Lim, and R. C. Giles, "Data encoding on terahertz signals for communication and sensing," *Opt. Lett.*, vol. 33, pp. 393–395, Feb. 2008.

[16] K. Kato, "Ultrawide-band/high-frequency photodetectors," *IEEE Trans. Microw. Theory Tech.*, vol. 47, no. 7, pp. 1265–1281, Jul. 1999.

[17] L. Y. Lin, M. C. Wu, T. Itoh, T. A. Vang, R. E. Muller, D. L. Sivco, and A. Y. Cho, "High-power high-speed photodetectors design, analysis, and experiment demonstration," *IEEE Trans. Microw. Theory Tech.*, vol. 45, no. 8, pp. 1320–1331, Aug. 1997.

[18] S. Demiguel, N. Li, X. Li, X. Zheng, J. Kim, J. C. Campbell, H. Lu, and A. Anselm, "Very high-responsivity evanescently coupled photodiodes integrating a short planar multimode waveguide for high-speed applications," *IEEE Photon. Technol. Lett.*, vol. 15, pp. 1761–1763, Dec. 2003.

[19] Y.-S. Wu, J.-W. Shi, P.-H. Chiu, and W. Lin, "High-performance dual-step evanescently-coupled uni-traveling-carrier photodiodes," *IEEE Photon. Technol. Lett.*, vol. 19, pp. 1682–1684, 2007.

[20] Y.-L. Huang and C.-K. Sun, "Nonlinear saturation behaviors of high-speed p-i-n photodetectors," *J. Lightw. Technol.*, vol. 18, pp. 203–212, Feb. 2000.

[21] H. Ito, S. Kodama, Y. Muramoto, T. Furuta, T. Nagatsuma, and T. Ishibashi, "High-speed and high-output InP-InGaAs unitraveling-carrier photodiodes," *IEEE J. Sel. Topics Quantum Electron.*, vol. 10, pp. 709–727, Jul./Aug. 2004.

[22] J.-W. Shi, Y.-T. Li, C.-L. Pan, M. L. Lin, Y. S. Wu, W. S. Liu, and J.-I. Chyi, "Bandwidth enhancement phenomenon of a high-speed GaAs-AlGaAs based unitraveling carrier photodiode with an optimally designed absorption layer at an 830 nm wavelength," *Appl. Phys. Lett.*, vol. 89, pp. 053512–, 2006.

[23] Y.-T. Li, J.-W. Shi, C.-Y. Huang, N.-W. Chen, S.-H. Chen, J.-I. Chyi, and C.-L. Pan, "Characterization of sub-THz photonic-transmitters based on GaAs/AlGaAs uni-traveling carrier photodiodes and substrate-removed broadband antennas for impulse-radio communication," *IEEE Photon. Technol. Lett.*, vol. 20, pp. 1342–1344, Aug. 2008.

[24] X. Li, N. Li, S. Demiguel, X. Zheng, J. C. Campbell, H. H. Tan, and C. Jagadish, "A partially depleted absorber photodiode with graded doping injection regions," *IEEE Photon. Technol. Lett.*, vol. 16, pp. 2326–2328, Oct. 2004.

[25] J.-W. Shi, H.-C. Hsu, F.-H. Huang, W.-S. Liu, J.-I. Chyi, J.-Y. Lu, C.-K. Sun, and C.-L. Pan, "Separated-transport-recombination p-i-n photodiode for high-speed and high-power performance," *IEEE Photon. Technol. Lett.*, vol. 17, pp. 1722–1724, Aug. 2005.

[26] S. Gupta, J. F. Whitaker, and G. A. Mourou, "Ultrafast carrier dynamics in III-V semiconductors grown by molecular-beam epitaxy at very low substrate temperatures," *IEEE J. Quantum Electron.*, vol. 28, no. 10, pp. 2464–2472, Oct. 1992.

[27] Y.-T. Li, J.-W. Shi, C.-L. Pan, C.-H. Chiu, W.-S. Liu, N.-W. Chen, C.-K. Sun, and J.-I. Chyi, "Sub-THz photonic-transmitters based on separated-transport-recombination photodiodes and a micromachined slot antenna," *IEEE Photon. Technol. Lett.*, vol. 19, pp. 840–842, Jun. 2007.

[28] Y.-C. Liang and N.-W. Chen, "An ultra-broadband coplanar waveguide-fed circular monopole antenna," presented at the EuCAP 2007, Edinburgh, U.K., Nov. 2007.

[29] G. M. Rebeiz, "Millimeter-wave and terahertz integrated circuit antennas," *Proc. IEEE*, vol. 80, pp. 1748–1770, 1992.

[30] N. Zamdmer, Q. Hu, K. A. Mclntosh, and S. Verghese, "Increase in response time of low-temeprature-grown GaAs photoconductive switches at high voltage bias," *Appl. Phys. Lett.*, vol. 75, pp. 2313–2315, Oct. 1999.

[31] J.-W. Shi, K. G. Gan, Y.-H. Chen, C.-K. Sun, Y. J. Chiu, and J. E. Bowers, "Ultra-high power-bandwidth product and nonlinear photo-conductance performances of low-temperature-grown GaAs based metal-semiconductor-metal traveling-wave photodetectors," *IEEE Photon. Technol. Lett.*, vol. 14, pp. 1587–1589, Nov. 2002.

[32] M. Tani, S. Matsuura, K. Sakai, and S. Nakashima, "Emission characteristics of photoconductive antennas based on low-temperature-grown GaAs and semi-insulating GaAs," *Appl. Opt.*, vol. 36, pp. 7853–7859, Oct. 1997.

[33] J. P. Ibbetson and U. K. Mishra, "Space-charge-limited currents in nonstoichiometric GaAs," *Appl. Phys. Lett.*, vol. 68, pp. 3781–3783, 1996.

[34] J.-W. Shi and C.-W. Liu, "Design and analysis of separate- absorption-transport-charge-multiplication traveling-wave avalanche photodetectors," *J. Lightw. Technol.*, vol. 22, pp. 583–1590, Jun. 2004.

[35] J.-W. Shi and C.-K. Sun, "Design and analysis of long absorption length traveling wave photodetector," *J. Lightw. Technol.*, vol. 18, pp. 2176–2187, Dec. 2000.

[36] H. Togo, A. Sasaki, A. Hirata, and T. Nagatsuma, "Characterization of millimeter-wave antenna using photonic measurement techniques," *RF Microw. Comput.-Aided Eng.*, vol. 14, no. 3, pp. 290–297, Apr. 2004.

[37] A. Hirata, T. Furuta, H. Ito, and T. Nagatsuma, "10-Gb/s millimeter-wave signal generation using photodiode bias modulation," *J. Lightw. Technol.*, vol. 24, no. 4, pp. 1725–1731, Apr. 2006.

[38] Y.-S. Wu, N.-W. Chen, and J.-W. Shi, "A W-band photonic transmitter/mixer based on high-power near-ballistic uni-traveling-carrier photodiode (NBUTC-PD)," *IEEE Photon. Technol. Lett.*, vol. 20, pp. 1799–1801, Nov. 2008.

[39] E. Ivanov, S. Diddams, and L. Hollberg, "Study of the excess noise associated with demodulation of ultra-short infrared pulses," *IEEE Trans. Ultrason., Ferroelectr., Freq. Contr.*, pp. 1068–1074, 2005.

Yu-Tai Li received the M.S. degree in electrophysics in 2004 from National Chiao Tung University, Hsinchu, Taiwan, where he is currently working toward the Ph.D. degree in the Department of Photonics (DOP) and Institute of Electro-Optical Engineering (IEO).

His current research interests in THz photonics including THz emitters and their application in communication.

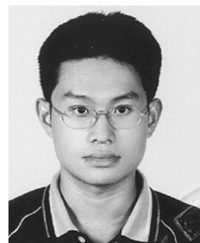

Jin-Wei Shi (M'02) was born in Kaohsiung, Taiwan, on January 22, 1976. He received the B.S. degree in electrical engineering from National Taiwan University, Taipei, Taiwan, in 1998 and the Ph.D. degree from the Graduate Institute of Electro-Optical Engineering of National Taiwan University, Taipei, Taiwan, in 2002.

He was a Visiting Scholar at the University of California, Santa Barbara, during 2000 and 2001. In 2002–2003, he served as a post-doc researcher at Electronic Research and Service Organization (ERSO) of Industrial Technology Research Institute (ITRI). In 2003, he joined the Department of Electrical Engineering, National Central University, Taoyuan, Taiwan, where he is now an Associate Professor. His current research interests include ultrahigh speed/power optoelectronic devices, such as photodetectors, electro-absorption modulator, sub-millimeter wave photonic transmitter, and semiconductor laser. He has authored or co-authored more than 60 journal papers and 100 conference papers, and holds 13 patents.

Dr. Shi was the invited speaker of 2002 IEEE LEGS, 2005 SPIE Optics East, 2007 AMWP, and 2008 AOE. He served as the technical program committee of OFC 2009 and 2010. He was the recipient of year 2007 Excellence Young Researcher Award from Association of Chinese IEEE.

C.-Y. Huang was born in Taoyuan, Taiwan, on November 3, 1982. He received the Master degree in electrical engineering from National Central University, Taoyuan, Taiwan, in 2008.

His current research interests include high-speed 850 nm photonic transmitter. He has authored or co-authored more than two journal papers and four conference papers.

Nan-Wei Chen received the B.S. degree in atmospheric sciences and the M.S. degree in space sciences from National Central University, Jhongli, Taiwan, in 1993 and 1995, respectively. He received the Ph.D. degree in electrical engineering at the University of Illinois at Urbana-Champaign, Urbana-Champaign, in 2004.

From 1998 to 2004, he was a Research Assistant at the Center for Computational Electromagnetics, University of Illinois, where he worked on time-domain integral equation methods for the solution of scattering and radiation problems. Since 2004, he has been an Assistant Professor of electrical engineering at the National Central University, Taiwan. His research interests include computational electromagnetics with special emphasis on time-domain integral equations, periodic structures, and millimeter-wave antennas.

Shu-Han Chen (M'03) was born in Hsinchu, Taiwan, on March 21, 1978. He received the B.S. degree and the Ph.D. degree in electrical engineering from the National Central University, Taiwan, in 2000, and 2008, respectively.

He is currently a Postdoctoral Fellow with the Research Center for Applied Science, Academia Sinica, Taipei, Taiwan. His current research includes molecular beam epitaxial (MBE) growth of InP-based heterojunction bipolar transistors, Sb-based material growth and high-speed electronic devices.

Jen-Inn Chyi (M'94–SM'98) received the B.S. and M.S. degrees in electrical engineering from National Tsing-Hua University, Hsin-Chu, Taiwan, R.O.C., in 1982 and 1984, respectively, and the Ph.D. degree in electrical engineering from the University of Illinois, Urbana-Champaign, in 1990. His Ph.D. dissertation dealt with molecular beam epitaxial (MBE) growth and characterization of InSb on GaAs.

In 1991, he joined the Department of Electrical Engineering, National Central University, Jhongli, Taiwan. Since then, he has established MBE, metal-organic vapor phase epitaxy (MOVPE), and high-speed optoelectronic devices laboratories, which house growth and characterization facilities for various III-V materials and devices. He was the Director of Optical Sciences Center of the University in 2000 to 2007. He is currently Dean of the College of Electrical Engineering and Computer Science, and Chair Professor of electrical engineering. His research interests are in the areas of MBE and MOVPE growth of III-V semiconductors and their heterostructures for high-speed electronic and optoelectronic devices. His current research projects include MBE growth of InP-based heterojunction bipolar transisters, quantum dot photonic devices, MOVPE growth of GaN-based materials for ultraviolet, blue, green emitters and high temperature, high power devices. He has authored or co-authored over 250 journal papers and has been granted 14 patents.

Dr. Chyi is the recipient of the 1996 Distinguished Young Researcher Award of the Electronic Devices and Materials Association of R.O.C. and the 2002 Distinguished Research Award of the National Science Council of R.O.C. He was awarded the Distinguished Professor of the Chinese Institute of Electrical Engineering in 2004. He also serves as a Distinguished Lecturer of IEEE EDS since 2004. He is an Associate Editor of IEEE PHOTONICS TECHNOLOGY LETTERS as well as the *Japanese Journal of Applied Physics*. He is a senior member of IEEE and a member of Phi Tau Phi.

Yi-Chao Wang received the Ph.D. degree in electro-optical engineering from National Chiao Tung University (NCTU), Hsinchu, Taiwan, in 2007.

He has been a Postdoctoral Fellow in the Department of Photonics and Institute of Electro-Optical Engineering, NCTU, since 2008. His research interests are ultrafast laser applications in semiconductor processing, ultrafast and THz photonics.

Chan-Shan Yang received the Bachelor degree in engineering from the Institute of Electro-Optical Engineering, National Chiao Tung University, Hsinchu, Taiwan, in 2007.

He is currently Master, Department of Photonics (DOP) and Institute of Electro-Optical Engineering, National Chiao Tung University, Hsinchu, Taiwan. His research interests are ultrafast lasers and their applications in THz photonics, optical communication and physical properties of liquid crystals.

Ci-Ling Pan (M'88–SM'03) received the Ph.D. degree in physics from Colorado State University, Ft. Collins, in 1979.

He is currently Tsing Hua Chair, Department of Physics, National Tsing Hua University (NTHU), Hsinchu, Taiwan. Prior to joining NTHU in February 2009, he was University Chair Professor, the Department of Photonics (DOP) and Institute of Electro-Optical Engineering (IEO), National Chiao Tung University (NCTU), Hsinchu, Taiwan. Prof. Pan was the director of IEO, NCTU (1992–1995), founding Chair of the DOP (2004–2006). He has also taken sabbatical leaves at the University of California, Berkeley, CA, Osaka University and the Chinese University of Hong Kong. The research interests of Prof. Pan are lasers and their applications in broadband optical communication, precision metrology, ultrafast and THz photonics. In particular, his group has recently developed numerous devices for laser and THz photonics with liquid crystal enabled functionalities.

Prof. Pan is a member of the Phi Tau Phi Honor Society (1991), a Fellow of the Photonic Society of Chinese Americans (1998); OSA, the Optical Society (2004), SPIE, the International Society of Optical Engineering (2004); and the Physical Society of Republic of China (2005). He was presented Merit Research Fellow Award of the National Science Council (2002), the Academics Award of the Ministry of Education (2004), the Engineering Medal by the Optical Engineering Society, Taiwan, R.O.C. (2004), Outstanding Engineering Professor Award of the Chinese Institute of Engineers (2006) and the Pan Wen Yuan Foundation Research Excellence Award (2007).